AJNR

A New Understanding of Dorsal Dysraphism with Lipoma (Lipomyeloschisis): Radiologic Evaluation and Surgical Correction

Thomas P. Naidich, David G. McLone and Saffet Mutluer

AJNR Am J Neuroradiol 1983, 4 (2) 103-116
http://www.ajnr.org/content/4/2/103

A New Understanding of Dorsal Dysraphism with Lipoma (Lipomyeloschisis): Radiologic Evaluation and Surgical Correction

Thomas P. Naidich[1]
David G. McLone[2]
Saffet Mutluer[2, 3]

The spinal anomaly designated dorsal dysraphism with lipoma (lipomyeloschisis) consists of skin-covered, focal spina bifida; focal partial clefting of the dorsal half of the spinal cord; continuity of the dorsal cleft with the central canal of the cord above (and occasionally below) the cleft; deficiency of the dura underlying the spina bifida; deep extension of subcutaneous lipoma through the spina bifida and the dural deficiency to insert directly into the cleft on the dorsal half of the cord; variable cephalic extension of lipoma into the contiguous central canal of the cord; and variable ballooning of the subarachnoid space to form an associated meningocele. The variable individual expressions of the anomaly are best understood by reference to their archetypal concept. Careful analysis of radiographic and surgical findings in human lipomyeloschisis and correlation with an animal model of lipomyeloschisis indicate that plain spine radiographs and high-resolution metrizamide computed tomographic myelography successfully delineate the precise anatomic derangements associated with lipomyeloschisis and provide the proper basis for planning surgical therapy of this condition.

Spinal lipomas are distinct collections of fat associated with an abnormally large amount of connective tissue; they appear at least partially encapsulated, and have a definite connection with the leptomeninges or spinal cord [1].

Intradural lipoma and lipomyelomeningocele are two forms of lipomyeloschisis (dorsal dysraphism with lipoma) [2–41]. Analysis of a series of 14 patients suggests that these conditions may be understood most easily in terms of variations about an archetype of the anomaly. Display of the specific anatomic derangements at every level by high-resolution transverse metrizamide computed tomographic (CT) myelography provides an important basis for planning corrective surgery and for assessing both operative risk and the likelihood of successful outcome.

Materials and Methods

The study material includes the presurgical plain spine radiographs, routine metrizamide myelograms, and metrizamide CT myelograms from each of 14 patients with lipomyeloschisis. There were 11 females and three males. Six patients were between 1 month and 1 year of age. Seven were 2–12 years old, and one was 35 years old. The lipoma was situated precisely in the midline in two patients and extended asymmetrically away from the midline in 10 patients (to the left: seven; to the right: three). In two other patients, the site of lipoma could not be determined because of prior surgery. One patient had a skin tag associated with the lipoma.

Five of the 14 patients had prior partial surgical correction of the superficial *extra*dural component of the lipomyelomeningocele. All 14 patients underwent subsequent definitive surgery, at which time surgical observations were recorded, and intraoperative photographs of the surgical dissection were obtained to document the correlation between radiography and in vivo anatomy. The final diagnoses were lipomyelomeningocele (seven patients), intradural lipoma (two), and lipomyeloschisis (exact nature obscured by partial prior treatment) (five).

This article appears in the March/April 1983 issue of *AJNR* and the June 1983 issue of *AJR*.

Received June 14, 1982; accepted after revision October 16, 1982.

Presented at the annual meeting of the American Society of Neuroradiology, Chicago, April 1981.

[1] Department of Radiology, Northwestern University Medical School, and Children's Memorial Hospital, 2300 Children's Plaza, Chicago, IL 60614. Address reprint requests to T. P. Naidich.

[2] Department of Neurosurgery, Children's Memorial Hospital and Northwestern University Medical School, Chicago, IL 60614.

[3] Present address: Department of Neurosurgery, Ege University Medical School, Bornova, Izmir, Turkey.

***AJNR* 4:103–116, March/April 1983**
0195-6108/83/0402-0103 $00.00

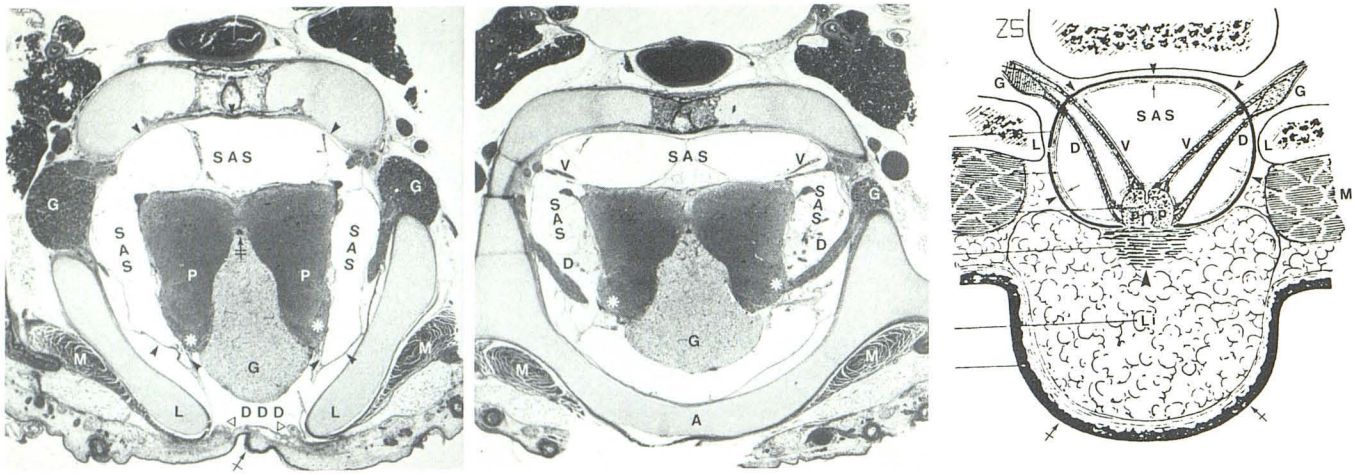

A B C

Fig. 1.—Cross-sectional anatomy. **A** and **B**, Axial sections of 21-day-old myeloschistic chicken embryo with dorsal glycogen body. Myelin stain. Ventral lies toward top. Relations of normal avian lumbosacral glycogen body and dura depicted here are believed to be a paradigm for human lipomyeloschisis. **A**, Intact skin (*single crossed arrow*) covers spina bifida. Bifid laminae (L) are joined by fibrovascular band (*open arrowheads*). Dura (*closed arrowheads*) underlies entire inner surface of vertebral canal *except* directly beneath spina bifida. Instead of crossing under spina bifida, dura is reflected onto posterolateral aspect of placode (P) at ipsilateral dorsal nerve root entry zone (*asterisks*), leaving a median dorsal dural deficiency (DDD). Left and right halves of neural tissue are joined only ventral to remnant of central canal (*double crossed arrow*) of spinal cord. Ventral surface of placode is lined by pia mater, which is continuous with arachnoid mater at dorsal root entry zones. Subarachnoid space (SAS) is crossed by multiple arachnoid trabeculae. Normal avian glycogen body (black G) occupies midline between dorsal halves of placode and projects posterior to neural tissue within dorsal dural deficiency. White Gs and Ms indicate dorsal root ganglia and paraspinal musculature, respectively. **B**, 5 mm cephalad. Intact neural arch (A). Paired ventral (V) and dorsal (D) nerve roots arise from pial surface of neural tissue. Glycogen body ascends within dorsal deficiency to underlie intact laminae of more cephalic vertebra. Glycogen body only appears to be intradural at this level. **C**, Anatomic relations in human lipomyeloschisis. Ventral at top. Dura (*small arrowheads*), placode (P), and subarachnoid space (SAS) extend out of spinal canal between the bifid laminae (L). Dura inserts onto placode just dorsal to entry of dorsal nerve roots (D). Pia-arachnoid forms single continuous membrane which lines dura and is reflected over ventral surface of placode. Skin (*crossed arrows*) is intact. Subcutaneous lipoma (Li) inserts onto dorsal face of lipoma via fibrous subareolar layer (*large arrowhead*). G = dorsal root ganglion; M = paraspinal muscle. (Reprinted from [22].)

In each patient, preoperative myelography was performed in the decubitus position with the lipoma side dependent via lateral C1–C2 puncture monitored by vertical-beam fluoroscopy using metrizamide in a concentration of 190–220 mg I/ml. About 2 hr after myelography, each patient underwent CT using an EMI 5005 general scanner. In 11 of the 14 patients, CT was performed with the high-resolution sector scan modification [42], using contiguous 5-mm-thick axial sections, 25.4 cm wedges, 140 kVp, 28 mA, and 70 sec scan time. Direct coronal images and computer reformatted coronal and sagittal images were obtained in selected cases.

Surgical and radiographic data were then correlated with the anatomic derangements observed in myelin-stained transverse sections of chicken embryos in which spina bifida was induced by dorsal midline incision of the caudal spine and neural tube at 72–90 hr after fertilization (just after closure of the posterior neuropore); the embryos were sacrificed at term (21 days) (fig. 1) [43–47]. Details of this technique for inducing myeloschisis and the results of that study are to be the subject of a separate report.

Anatomic Relations in Lipomyeloschisis

Dossetor et al. [9], James and Oliff [14], Kaiser et al. [17], Kaplan and Quencer [18], Lohkamp et al. [23], Resjo et al. [30], Scatliff et al. [33], Schroeder et al. [34], and Wolpert et al. [40] have contributed to our understanding of the CT appearance of dorsal dysraphism with lipoma. Bulcke et al. [48], Osborn and Koehler [49], Chiu and Schapiro [50], and Schapiro and Chiu [51] have contributed to our understanding of the CT appearance of the paraspinal musculature. On the basis of our experience with high-resolution CT and correlation with surgical findings, we present an *archetype* of lipomyeloschisis against which the details of each individual may be viewed as variations on a theme (fig. 1).

Patients with dorsal dysraphism and lipoma typically exhibit a subcutaneous soft-tissue mass that occupies the midline and usually extends asymmetrically toward one side. Deep to this mass is a relatively focal spina bifida that usually involves the lumbosacral spine. The transition from normal to bifid vertebrae may be abrupt or gradual. A thick fibrovascular band joins the laminae of the most cephalic vertebra with widely bifid laminae. Patients in whom a normal spinal canal reforms below the spina bifida frequently exhibit a fibrovascular band joining the laminae of the most caudal vertebra with widely bifid laminae as well. The band is continuous with the periosteum of the laminae. The bands are not present in the center of the spina bifida, and appear to be transitional elements that roof-over the canal at the cranial and caudal ends of the spina bifida.

In patients with lipomyelomeningocele, the meningocele and spinal cord herniate posteriorly into the subcutaneous tissue under the fibrovascular band (NOT under the last intact arch nor under narrowly bifid laminae). The fibrovascular band kinks and notches the superior surface of the spinal cord and meningocele in all cases of lipomyelomeningocele. This band appears to tether the meningocele sac and neural tissue, since they relax after surgical section of this band, and since, in at least some cases, cortical-evoked

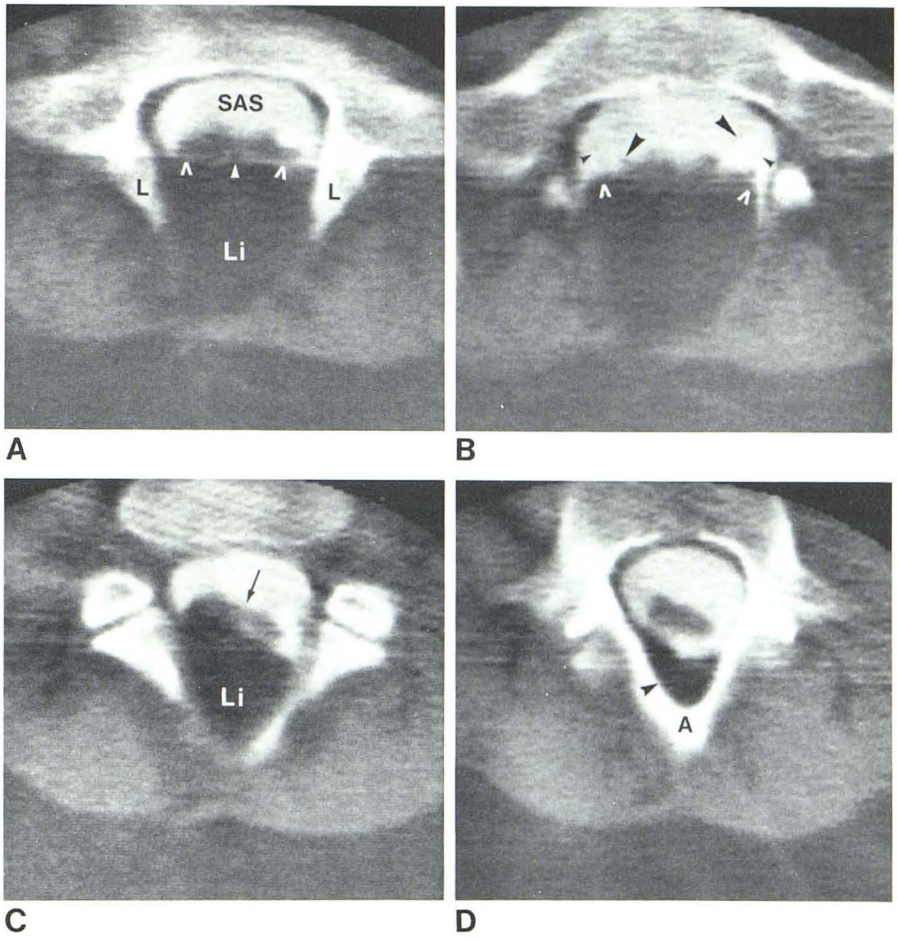

Fig. 2.—Lipomyeloschisis in 10-year-old girl with previous, purely extradural repair of lipomyeloschisis. **A** and **B**, Axial section metrizamide CT. Bifid laminae (L); lucent dorsal lipoma (Li); ventral pial surface facing opacified subarachnoid space (SAS); paired dorsal (*small black arrowheads*) and ventral (*large black arrowheads*) nerve roots arise from placode to course through subarachnoid space; smooth, apparently distinct lipal/neural interface at dorsal surface of placode (*open white arrowheads*); dorsal midline notch (*solid white arrowhead*) is believed to represent residual neural groove; junction of lateral borders of placode, lipoma, and subarachnoid space along dorsal root entry zones (*open white arrowheads*). Shape of placode is strikingly similar to shape of neural tissue of chicken embryo at level of glycogen body (cf. figs. 1A and 1B). Subarachnoid space bulges slightly posterolaterally to dorsal root entry zones. **C**, Lipoma (Li) ascends along posterior surface of placode, rotates placode (*arrow*), and then, **D**, separates from neural tissue to form extraarachnoid dorsal fat pad (*arrowhead*) under intact arch (A) of next cephalic vertebra. Degree of rotation of cord and placode varies from level to level.

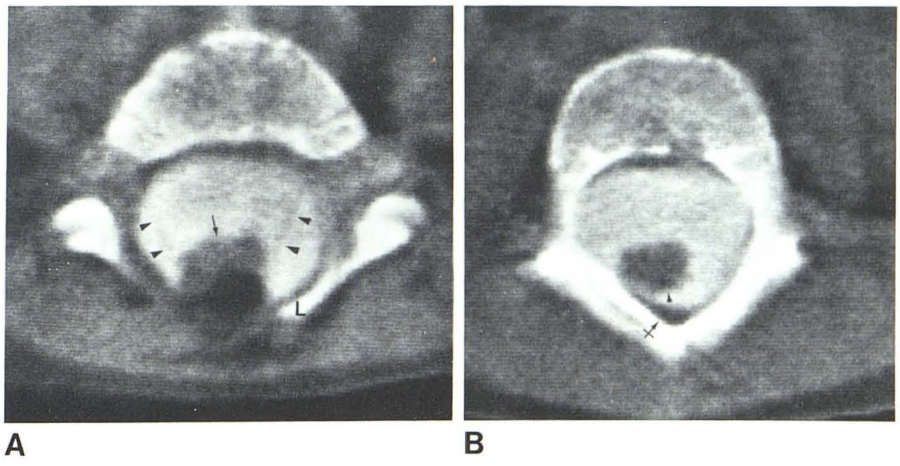

Fig. 3.—3-year-old girl with previous partial repair of lipomyelomeningocele. **A**, Axial section metrizamide CT at level of bifid laminae (L) discloses opacified subarachnoid space; characteristically shaped, isodense, slightly rotated placode (*arrow*) giving rise to paired dorsal nerve roots (*arrowheads*); smooth, distinct lipal/neural interface; and lucent dorsal lipoma with spikelike anterior extension along neural groove. Conjunction of subarachnoid space, placode, and lipoma marks dorsal root entry zone on each side. Subarachnoid space bulges slightly posterior to placode. **B**, 2 cm cephalad. Ascent of lucent lipoma (*arrowhead*) along dorsal face of placode and within epiarachnoid (presumably epidural) space (*arrow*) to underlie intact vertebral arch.

potentials recorded from posterior tibial nerve electrodes show increased amplitude and decreased latency after section of the band. Caudal fibrovascular bands usually kink the inferior surface of the meningocele as well. The site of the fibrovascular band, the site of the superior kink in the meningocele sac, and the point of herniation may usually be predicted on plain radiography and CT by identifying the level of the most cephalic, widely bifid laminae.

The spinal cord and conus lie low in position and are split in the midline dorsally (partial dorsal myeloschisis) (figs. 2 and 3). As a result, the caudal neural tissue retains the shape of the embryonal neural placode and is designated

hereinafter the placode. The dorsal myeloschisis is typically present at the level of the spina bifida and may extend superiorly to underlie the intact spinal arches of more cephalic vertebrae (fig. 2C). Because of the myeloschisis, the nerve root origins lie nearly in the same coronal plane, with the dorsal roots situated lateral to the ventral roots (figs. 2A and 2B).

The points at which the dorsal roots enter the spinal cord (or placode) are termed the dorsal root entry zones. The dorsal root entry zones appear to lie at the lateralmost extent of the placode. Thus, the paired dorsal root entry zones at each level divide the surface of the placode into ventral and dorsal faces. The ventral face of the placode represents the outer surface of what should have been a closed neural tube, and is covered by pia mater. This ventral face fronts onto the subarachnoid space and the cerebrospinal fluid (CSF) it contains (figs. 1–3). The paired ventral and dorsal nerve roots emerge from the ventral face of the placode (not the lipoma) and traverse the subarachnoid space (not the lipoma) to reach their root sleeves and exit foramina. The dorsal face of placode represents the abnormal surface that should have formed the interior of the neural tube. The midline groove typically observed in the dorsal face of the placode represents the remnant of the embryonic neural groove and merges with the open central canal of the spinal cord cranially (figs. 2 and 3).

The dura that forms a closed tube within the normal spinal canal is deficient dorsally at the zone of spina bifida. At the spina bifida, the dura appears to be reflected onto the ipsilateral edge of the placode just dorsal to the entry zones of the dorsal roots. This leaves a dorsal dural deficiency or dehiscence (fig. 1). Because the dura is reflected onto the placode immediately dorsal to the dorsal roots, the entire dorsal face of the placode is, anatomically, outside the dural membrane. Thus, the subcutaneous lipoma may extend inward into the bifid spinal canal, and become intimately attached to the dorsal face of placode by passing through the dorsal dural deficiency. It does not invade through the dura.

In most cases, the lipoma expands the placode, dishes out its dorsal surface, and raises its edges, so the placode comes to resemble a Chinese soupspoon (fig. 4). In the uncomplicated case, the dorsal lipal/neural junction appears deceptively smooth and well defined on CT scans (figs. 2–4). The lipoma may extend upward along the myeloschisis to underlie the intact arches of more cephalic vertebrae (figs. 2 and 3). It may enter the open central canal of the spinal cord and pass upward to form apparently isolated "intradural" lipoma at higher levels. The lipoma may also extend into the spinal canal between the dura and the bony wall to form prominent dorsal and ipsilateral fat pads in the extradural space. Because lipomas most frequently enter the spinal canal at a very low level and then ascend within the canal, continuity between the intracanalicular and extracanalicular components of the mass can be documented only by tracing serial images far caudally (figs. 2 and 4).

The normal epidural fat is anatomically distinct from the lipoma itself and appears looser and more areolar at surgery. Only at the caudalmost extent of sacral lipomas does the lipoma merge with intracanalicular sacral fat. Nerves should normally be seen in the epidural fat. These represent peripheral nerves that have already exited from the subarachnoid space. They are not roots of the cauda equina entrapped within lipoma.

The inner surface of the dura is lined by the arachnoid. This is directly continuous with the pia mater that covers the ventral face of placode (figs. 1 and 2). The pia and arachnoid, in fact, represent a single continuous membrane with identical histology and are better termed "pia-arachnoid." The entire pia-arachnoid sac is contained within the dural sac, and like the dural sac, ends at the dorsal root entry zones (figs. 1–4). The lipoma, therefore, also lies entirely outside the pia-arachnoid sac; it does not invade the pia-arachnoid to enter the subarachnoid space. The dorsal lipoma, ventral subarachnoid space, and placode meet at the lateral edge of the placode along the paired dorsal root entry zones. On CT, then, the conjunction of CSF, fat, and neural tissue is a useful landmark for the dorsal root entry zones on each side (figs. 2, 3, and 5). The subarachnoid space may bulge into or lateral to the lipoma, posterior to the dorsal root entry zones, presumably because CSF pulsations balloon the subarachnoid space (figs. 4D–4H).

In patients with lipomyelomeningocele, it is probable that expansion of the spinal subarachnoid space ventral to the placode causes the placode, cord, arachnoid sac, and dura to herniate posteriorly [52]. The distal cord or the placode becomes kinked under the fibrovascular band stretched between the laminae of the most cephalic, widely bifid vertebrae. Because the lipoma is typically asymmetric and is intimately attached to the dorsal surface of placode, the lipoma tethers the placode as it herniates posteriorly and causes it to rotate its dorsal surface to the side of the lipoma (figs. 4 and 5). Such rotation and herniation often bring the contralateral dorsal roots and dorsal root entry zones into the midline, posterior to the protective laminae, where they are at increased risk for surgical trauma (fig. 6).

The meningocele typically balloons to the side opposite the lipoma (figs. 4 and 5). The expanding subarachnoid space thins and evaginates the herniating placode and, in effect, converts a portion of the placode into a thin, everted wall for the distended arachnoid sac (fig. 4). Electrophysiologic testing at surgery indicates that these thin portions give rise to *functional* nerve roots that cross the subarachnoid space within the meningocele and reenter the spinal canal before exiting their neural foramina (fig. 6). Preliminary data suggest that the meningocele does not expand progressively, since the size of the meningocele sac bears no constant relationship to age. Serial studies following one untreated patient over time are not available, however.

Radiographic Observations

Spina bifida was observed in 13 of the 14 cases. One patient with intradural lipoma exhibited segmentation anomalies of L5 and S1, without true spina bifida. The spina bifida extended upward from the coccyx in all 13 patients. The highest extent of the spina bifida *included* S1 in three

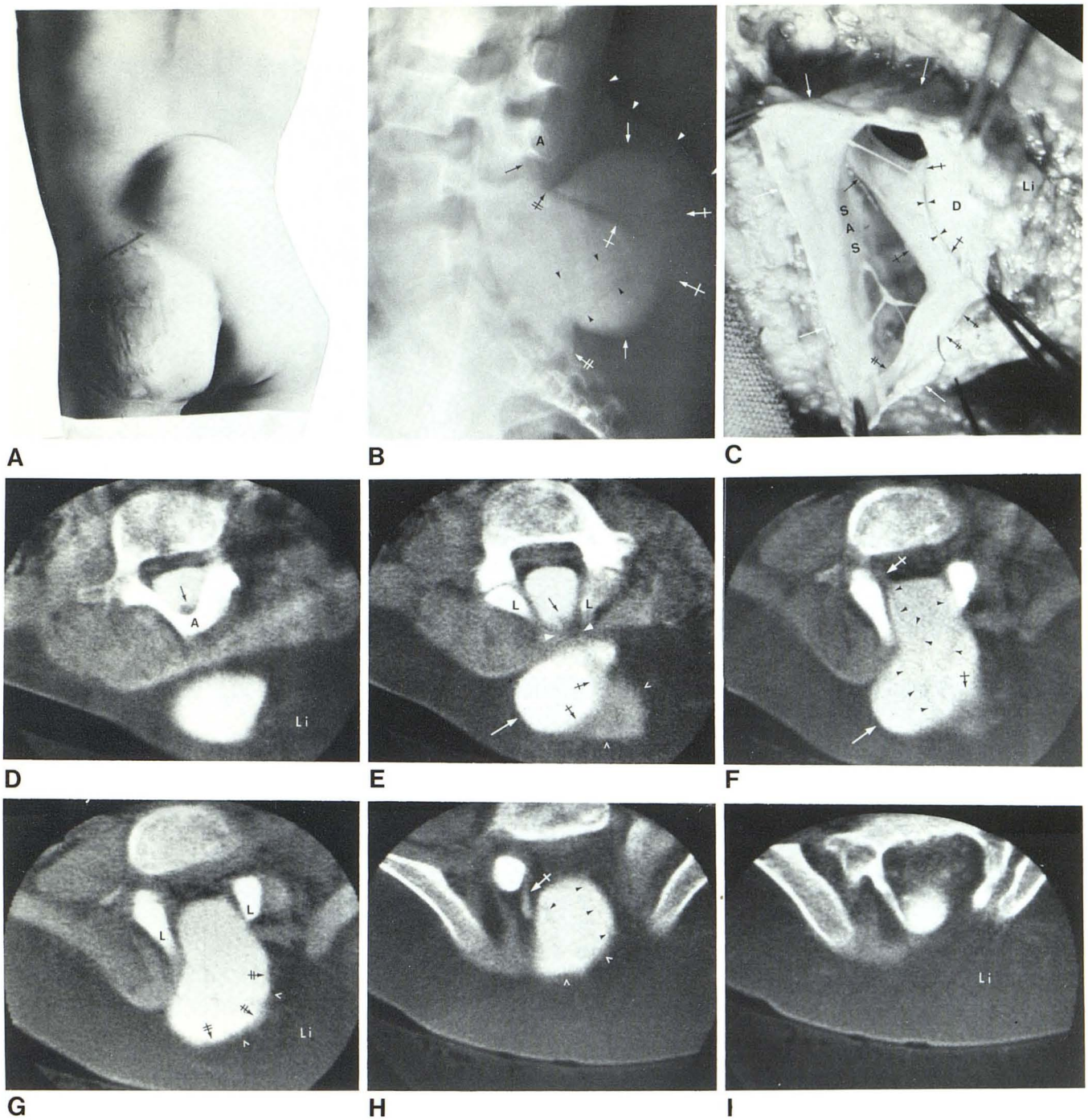

Fig. 4.—Lipomyelomeningocele, 12-year-old boy with left leg wasting, fecal incontinence, and grafted right buttock pressure sores. **A**, Scoliosis and asymmetric, skin-covered lumbosacral mass. **B**, Lateral metrizamide myelogram. Lipomatous mass (*white arrowheads*); thinned, tethered spinal cord (*uncrossed black arrow*) pulled tightly against last intact neural arch (A); herniation of cord into dorsal meningocele (*uncrossed white arrows*) well below that last intact arch at point corresponding to fibrovascular band (*double crossed black arrow*); widening of herniating cord into placode (*single crossed white arrows*) at posterior end of meningocele; nerve roots (*black arrowheads*) traverse opacified subarachnoid space to reenter spinal canal; sharp notching of meningocele at hernia ostium superiorly and inferiorly, and large extraarachnoid space (fat pad) behind vertebral bodies. Inferior point caudal to hernia ostium (*double crossed white arrow*). **C**, Different patient with comparable lipomyelomeningocele. Incision into large meningocele (*white arrows*) exposes subarachnoid space (SAS). Herniated spinal cord (*uncrossed black arrow*) widens and expands into deeply dished placode (*single crossed arrows*) which then evaginates and thins out (*double crossed arrows*) along section of meningocele wall. Lipoma (Li) lies entirely extraarachnoid and extends into dorsal surface of placode through dorsal dural deficiency, outside both arachnoid sac and dura mater (D). *Arrowheads* indicate both junction of placode with dura and point at which arachnoid mater is reflected from wall of sac onto ventral surface of placode, where it is termed pia mater. (Courtesy of Francisco Gutierrez, Chicago.) **D–I**, Metrizamide CT myelogram, serial 5 mm sections from cephalad to caudad. **D**, Asymmetric, skin-covered lipoma (Li) reaches just over midline. Thinned, tethered spinal cord (*arrow*) is pulled to inner aspect of last intact neural arch (A). Opacified sac bulges superiorly behind intact neural arch. **E–H**, Axial sections 5, 10, 15, and 30 mm inferior to **D**. Spinal cord (*uncrossed black arrow*) herniates through bifid laminae (L) under fibrovascular band (*closed white arrowheads*) into dorsal sac, and expands into placode (*single crossed black arrows*) which evaginates into thin "lining" (*double crossed arrows*) along wall of sac. Cord and dorsal face (*open white arrowheads*) of placode rotated to side of lipoma. Neural/lipal interface appears sharp and distinct. Meningocele (*white arrow*) bulges to contralateral side. Paraspinal muscles are asymmetrically smaller on side of lipoma and of wasted leg. Nerve roots (*black arrowheads*) arise from ventral surface of placode (not lipoma), and course through subarachnoid space back into spinal canal to enter their root sleeves (*crossed white arrow*) at neural foramina. **I**, Lipoma extends into spinal canal ipsilateral to subarachnoid space and then ascends within canal as large ventral fat pad.

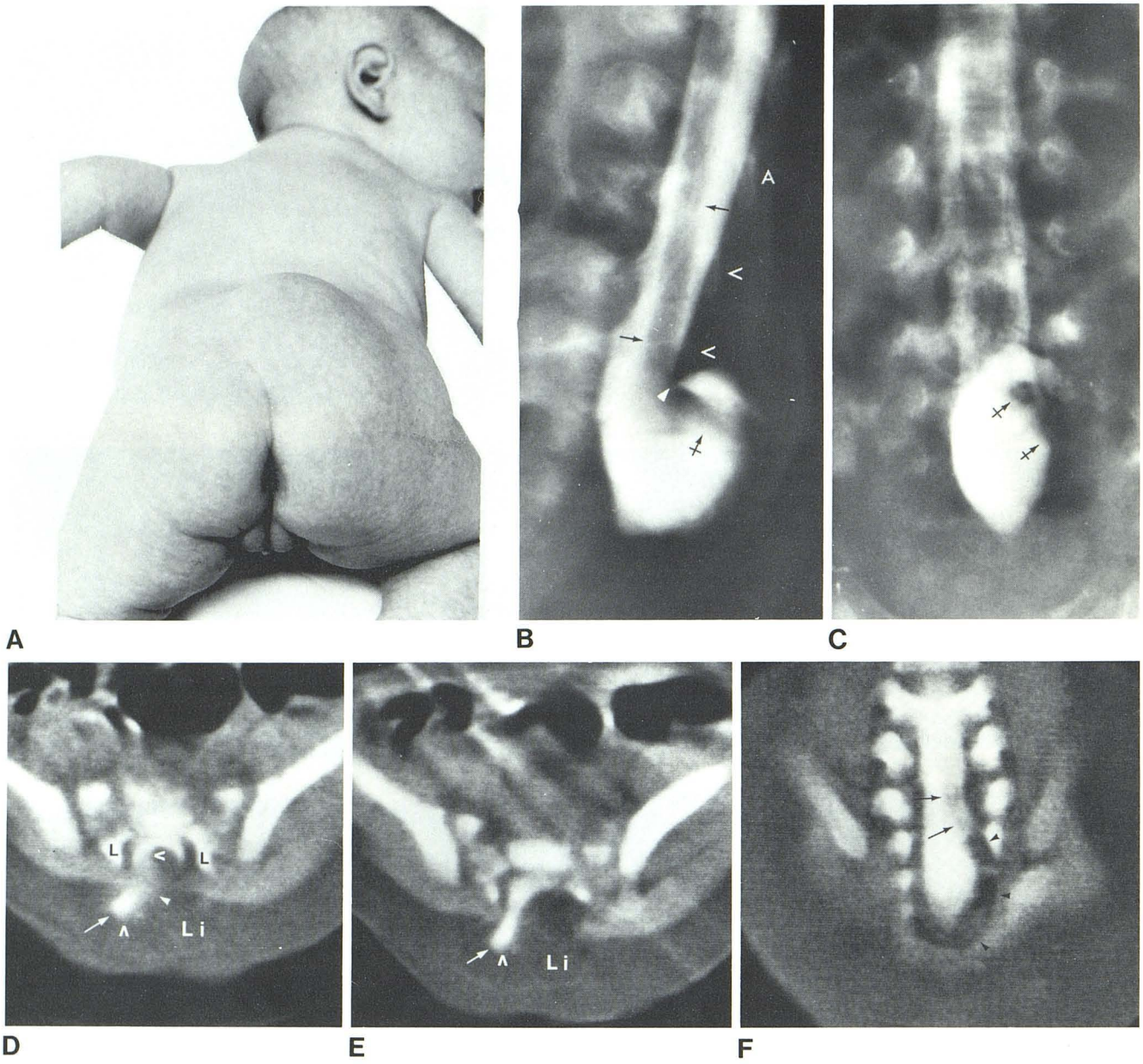

Fig. 5.—1-month-old girl with lipomyelomeningocele. **A**, Skin-covered lumbosacral mass at and to left of midline. **B**, Lateral metrizamide myelogram. Tethered cord (*uncrossed arrows*) herniates posteriorly (*crossed arrow*) into dorsal arachnoid sac. Sharp notching (*closed arrowhead*) of superior borders of sac and cord as they exit from spinal canal indicates site of fibrovascular band. In this patient, two segments with narrowly bifid laminae (*open arrowheads*) intervened between last intact vertebral arch (A) and fibrovascular band (apex of the notch). **C**, Anteroposterior metrizamide myelogram. Herniating cord (*arrows*) is pulled to side of asymmetric lipoma, while sac bulges to contralateral side. **D** and **E**, Axial metrizamide CT. Bifid spinal canal (L); lucent lipoma (Li); rotated, isodense placode (*closed arrowhead*) with smooth, distinct lipal/neural interface; and opacified arachnoid sac (*arrows*). Although individual nerve roots were too small to resolve, conjunction of opacified subarachnoid space, placode, and lipoma marked dorsal root entry zones (*open arrowheads*). Right dorsal root entry zones have been rotated into midline, posterior to laminae, where they are at increased risk of surgical trauma. **F**, Direct coronal metrizamide CT myelogram. Spinal cord (*arrows*) is pulled to side of lipoma (*arrowheads*) while sac bulges contrad.

patients, L5 in four patients, L4 in three patients, and L3 in three patients.

The laminae were asymmetrically shorter on the side of the lipoma in five of nine new cases and two of five reoperated cases. The laminae were nearly equal bilaterally in the rest. Three (21%) patients exhibited scoliosis. The scoliosis was concave toward the side of lipoma in two of the three, and concave away from the side of lipoma in the third case. Two cases manifested partial sacral defects and/or confluent neural foramina. One patient exhibited an anomalous dorsal bony keel articulating with the sacroiliac joint (fig. 7).

Asymmetrically small size of the paraspinal and gluteal

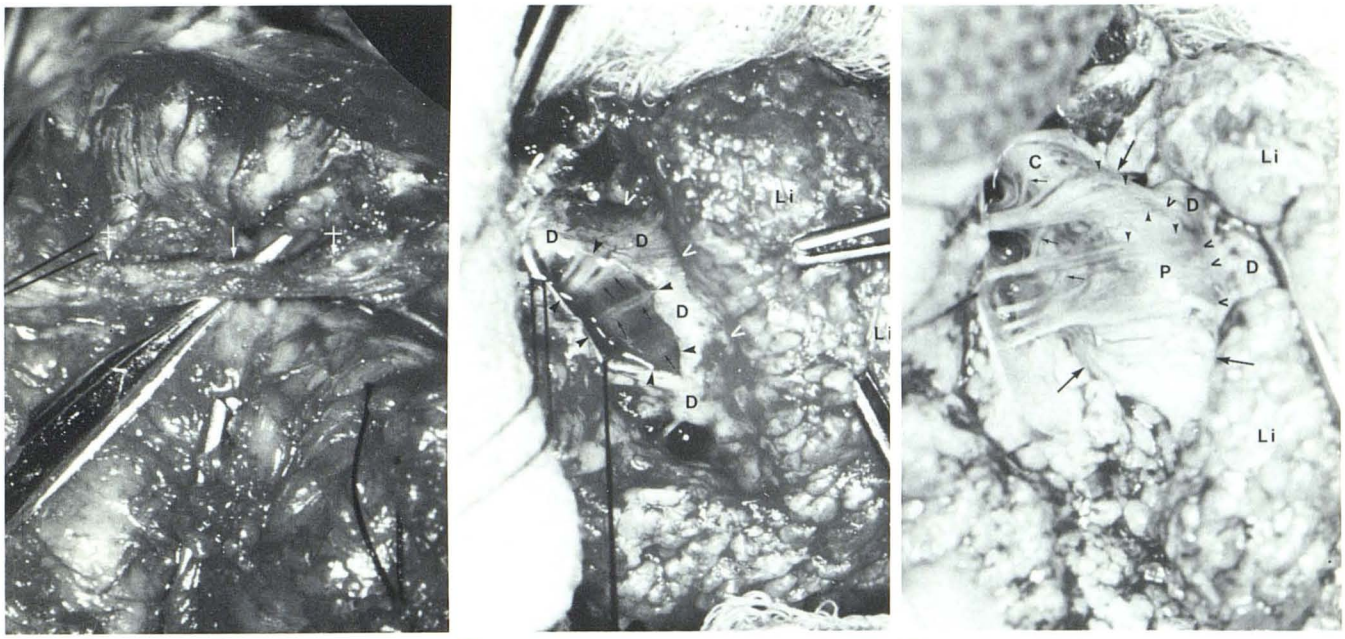

A B C

Fig. 6.—Intraoperative photographs illustrate surgical procedure. All images viewed from behind with cephalic toward top. **A**, Patient in fig. 8. With prior knowledge of vertebral segments, surgeon dissects downward to expose last intact vertebral arch. Palpation discloses medial edges of most cephalic, widely bifid laminae (*crossed arrows*) and tough fibrovascular band (uncrossed arrow) which crosses between them. Section of band untethers the dural tube and releases sharp kink in superior surface of meningocele. **B**, Patient in fig. 5. Operative field as seen from patient's right posterior aspect. Because entry into subarachnoid space is safest and easiest where sac is largest and because subarachnoid space characteristically bulges to side *opposite* lipoma, surgeon rotates lipoma (Li) ipsilaterally to expose side of meningocele and continues to dissect downward until he uncovers dura (D) over bulging subarachnoid space. Taking care not to injure dorsal roots at dorsal root entry zones (*white arrowheads*), surgeon then incises (*black arrowheads*) dura parallel to and well anterior to lipal/dural junction to expose intact, bulging, glistening arachnoid and course of nerve roots (*arrows*) deep to arachnoid in subarachnoid space. Generous cuff of dura left between lipal/dural junction and line of dural incision. **C**, Same patient, same orientation. Arachnoid is next incised under direct loupe magnification, carefully sparing roots themselves. Dural/arachnoid incisions are then extended around entire circumference of tethered conus to expose spinal cord (C) and expanded, spoon-shaped placode (P, between *large arrows*). *Deep* aspect of generous cuff of dura (D) lined by arachnoid mater which encompasses subarachnoid space. Deep surface of dural/lipal junction (*open arrowheads*). Lipoma (Li) lies entirely outside subarachnoid space; dorsal nerve roots (*closed arrowheads*) emerge entirely from placode, traverse subarachnoid space for substantial distance, and join together with ventral roots (*small arrows*) to exit canal at their root sleeves; lipal/dural junction lies at lateral edge of placode; lipal/dural junction and point of confluence of CSF, placode, and fat do, indeed, mark dorsal root entry zones; and rotation of placode has brought dorsal root entry zones into midline. Because cord is tethered and low-lying, there is no cauda equina. Cord and placode are now untethered and typically ascend within surgical field for a variable distance, often 1–2 cm. Lipoma is then trimmed as completely as possible, deliberately leaving behind some fat to avoid inadvertent injury to dorsal surface of placode. Any superior extension along dorsal surface of cord or within central canal is debulked as much as possible. Placode is reformed into closed neural tube. Dura is closed (or patch-grafted with fascia) and wound is closed.

musculature was observed ipsilateral to the lipoma in four of nine new and three of five reoperated cases (fig. 4). Definitely increased lucency of the ipsilateral paraspinal and gluteal musculature was observed in one of nine new cases, and questionably increased lucency of the musculature in another two of nine new and one of five reoperated cases. Asymmetrically enlarged gluteal musculature was observed ipsilateral to the anomalous bony keel, which offered unusually fine purchase for muscle attachment (fig. 7).

Definite asymmetric subcutaneous lipoma was observed in seven of nine new cases and four of five reoperated cases (fig. 4). Two new patients with "intradural" lipoma exhibited only minimal extracanalicular fat deposits which ran vertically in the midline deep to the paraspinal musculature. One reoperated patient had no residual extracanalicular fat. The extracanalicular mass could be traced in continuity into the spinal canal in all but one patient (fig. 4) whose meningocele was so large that the entire lipoma, lower spinal cord, and placode lay extracanalicularly. Asymmetric, extraarachnoid fatty deposits were observed along the ipsilateral border of the intracanalicular subarachnoid space in five of nine new cases and three of five reoperated cases (fig. 4).

The conus lay in low position in all 14 cases. The dorsally open placode was visualized in seven of nine new cases and four of five reoperated cases. The intracanalicular portion of the placode was dished out or expanded by fat in five of nine new and three of five old cases. Lipoma lay in intimate association with the dorsal surface of placode and cord in seven of nine new cases (i.e., all those with lipomyelomeningocele), and in four of five reoperated cases. In one of the five reoperated cases, there was virtually no residual fat. The interface between lipoma and the dorsal surface of the placode was very distinct and relatively smooth in five of seven new patients with lipomeningocele. The interface was very indistinct in one patient with complicating dermal/epidermal elements traversing the lipoma (fig. 8) and in one

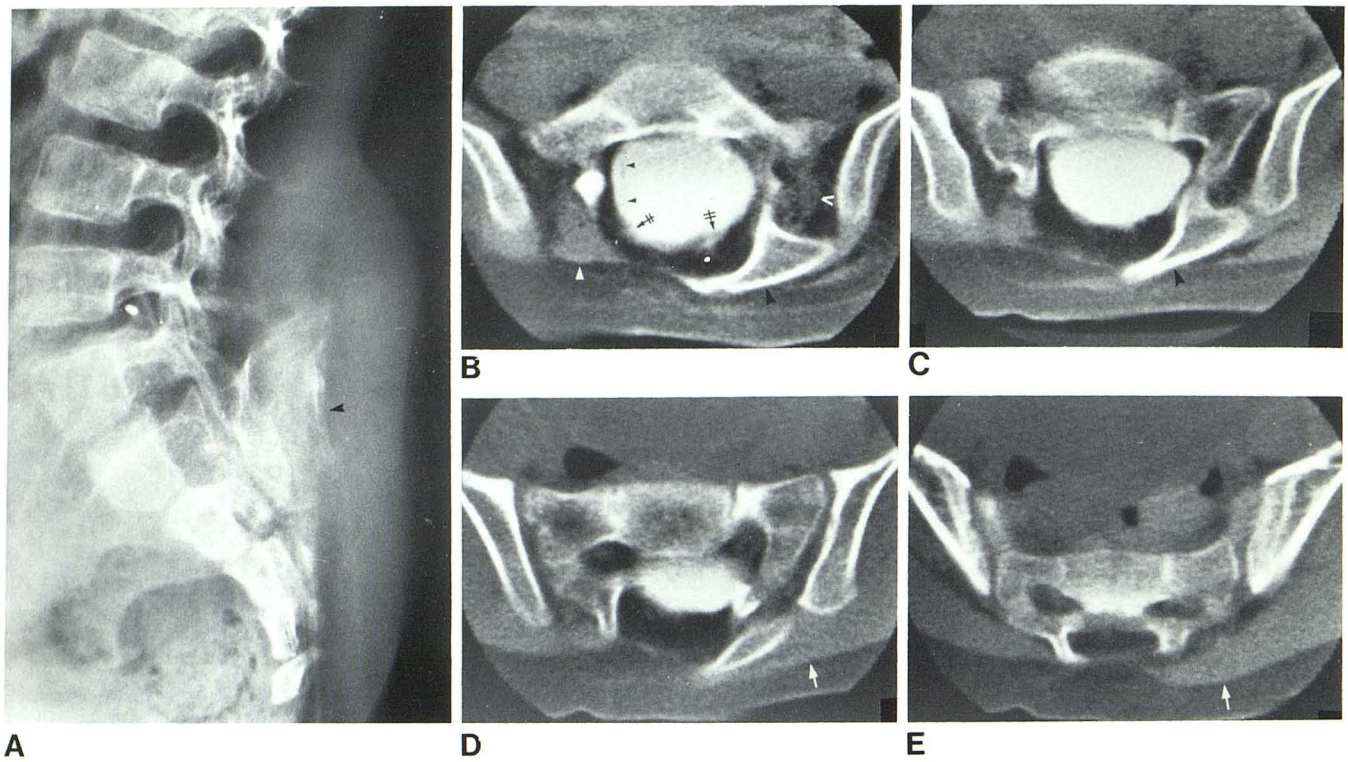

Fig. 7.—Anomalous bone at sacroiliac joint with consequent asymmetry of paraspinal musculature, 6-year-old girl with previous partial repair of lipomyelomeningocele. **A**, Lateral spine radiograph. Posterior lipoma and keellike bone (*arrowhead*) projecting into it. **B–E**, Serial metrizamide CT myelogram sections displayed from cephalad to caudad. Thinned placode (*black arrows*) gives off nerve roots (*small black arrowheads*) into subarachnoid space. Anomalous bone (*large black arrowhead*) articulates with both sacrum and iliac wing across asymmetrically widened sacroiliac joint. Compared with paraspinal muscles seen on opposite side (*closed white arrowhead*), paraspinal muscles on side of anomalous bone are poorly defined and fatty (*open white arrowhead*). Gluteus maximus (*white arrow*) is far larger and better defined on side of anomalous bone and inserts onto it.

patient with a *component* of the lipoma which grew upward within the central canal of the cord, ballooned it, and thinned the interface beyond recognition. In the two of nine new cases with "intradural lipoma," the large intracanalicular fat masses expanded and thinned the cord, preventing accurate assessment of the lipal/neural interface.

A portion of the neural tube herniated into the dorsal arachnoid sac in all seven cases with meningocele. In three of nine new cases, the whole placode herniated outside the canal into the meningocele. The placode and cord were displaced toward the side of asymmetric lipoma in six of nine new cases. In three new cases, large intracanalicular fat deposits appeared to prevent lateral displacement of cord. The placode was rotated in eight of nine new cases and four of five reoperated cases. The nerve roots were clearly shown to arise from placode in nine of 14 cases. The conjunction of lipoma, placode, and subarachnoid space definitely marked the dorsal root entry zones in two of nine new and three of five reoperated cases (figs. 2 and 3). In the others, this conjunction almost certainly marked the dorsal root entry zones, but dorsal and ventral roots could not both be shown in the same CT section to prove the point. The cerebellar tonsils lay in low position (C2) in one patient (fig. 9).

A dorsal meningocele was present and continuous with the intracanalicular subarachnoid space in seven of nine new cases and none of five reoperated cases. The meningocele was large in three of seven cases: ages 8 months, 11 months, and 2 years; modest in three of seven cases: ages 1 month, 11 months, and 3 years; and small in one of seven cases: age 5 months. In all seven patients: the meningocele lay lateral to the placode, bulged to the side opposite the lipoma, appeared to bulge into the lipoma, and exhibited a sharp or slightly blunted point at its caudal border. In six of seven cases, the meningocele projected superior to the placode in lateral views.

All seven meningoceles showed a distinct kink in the superior surface of the sac, where it passed under the fibrovascular band (figs. 4B, 5B, and 8C). The kink was sharp in six cases and modest in one. Kinks were also observed at the inferior margin of the hernia ostium in three meningoceles (fig. 4B) and at the lateral border of the hernia ostium in two meningoceles.

In all seven cases with meningocele, the most cephalic, widely bifid laminae marked *simultaneously*: the upper end of the hernia ostium, the kink in the superior surface of the meningocele, and the point of herniation of the spinal cord and/or placode into the meningocele. The last intact verte-

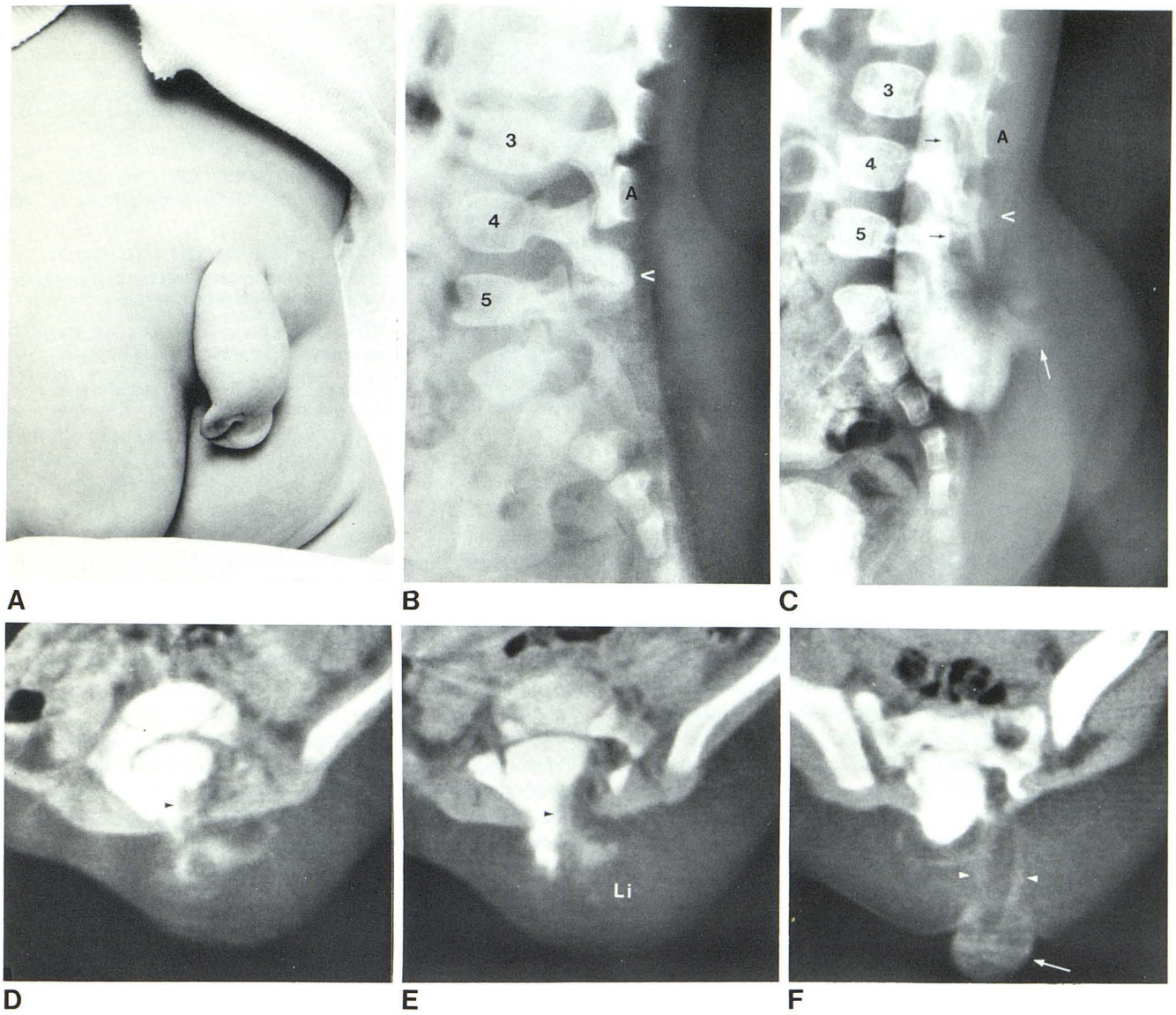

Fig. 8.—Lipoma with complicating skin appendage and dermal sinus, 11-month-old girl. **A**, Asymmetric, skin-covered lumbosacral mass with partially hollow skin appendage. By history, some "fluid" discharged from tail periodically. **B**, Last intact vertebral arch (A) is at L3 (3). L4 (4) arch (*arrowhead*) has partly formed laminae that do not fuse in midline. L5 (5) arch is most cephalic, widely bifid arch and likely site of herniation of meningocele and cord. **C**, Lateral metrizamide myelogram. Tethered cord (*black arrows*) and small arachnoid sac (*white arrow*) herniate posteriorly into lipoma at L5 level, under L5 fibrovascular band illustrated in fig. 6A. Narrowly bifid L4 arch (*arrowhead*) curves posterior to and indents subarachnoid space. No passage of metrizamide into skin appendage. **D**–F, Axial metrizamide CT scans exposed for lipal/dural junction. Asymmetric lucent lipoma (Li), spina bifida, opacified subarachnoid space, isodense placode (*black arrowheads*), and skin appendage (*white arrow*). Cutaneous elements of appendage extend deeply (*white arrowheads*) through lipoma to same side of spinal canal as lipoma itself. In this patient, unlike others, junction of lipoma with dorsal surface of placode is very irregular and difficult to define. **G**, Coned-down "root" image documents marked rotation and displacement of placode to side of lipoma. Contralateral ventral (V) and dorsal (D) nerve roots arise appropriately and pass to neural foramen. Ipsilateral ventral (*black arrowhead*) and faintly seen dorsal (*white arrowhead*) roots are extremely short at this level and could not be identified in most other sections. At surgery, basic derangements of lipomyeloschisis were as expected. However, dermal/epidermal elements extended deeply into spinal canal adjacent to placode, and short subarachnoid course of ipsilateral roots (prior to exiting neural foramen) bound cord tightly, preventing successful mobilization and untethering despite excision of lipoma and section of the filum.

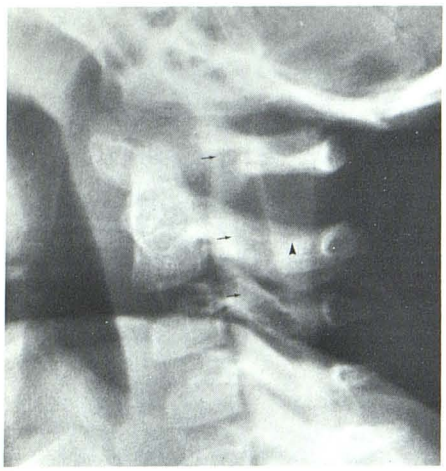

9

Fig. 9.—Lipomyeloschisis with Chiari I deformity. Lateral metrizamide myelogram, 2-year-old girl. Low-lying tonsils (*arrowhead*) posterior to cervical spinal cord (*arrows*) signify Chiari I deformity. This is the sole example of concurrent Chiari I malformation and lipomyeloschisis in our series.

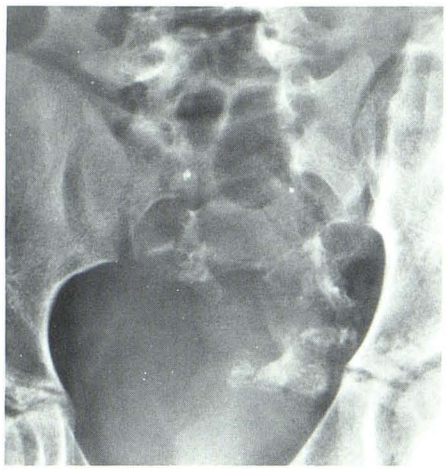

10

Fig. 10.—12-year-old girl with prior partial surgical correction of lipomyeloschisis. Plain frontal spine film discloses sacral scoliosis with sacral defect and confluent neural foramina. At surgery, unusually short subarachnoid courses of nerve roots ipsilateral to defect prevented complete mobilization and untethering of cord despite successful excision of lipoma.

bral arch exhibited a variable relation to the most cephalic, widely bifid laminae. Most often (four of seven patients), there was a gradual transition over three vertebrae (from above downward): a vertebra with intact or stubby spinous process, the next lower vertebra with narrowly bifid laminae that curved posterior to the canal but failed to fuse in the midline, and the still lower vertebra with widely bifid laminae. In these four patients, the upper end of the hernia ostium and point of cord herniation were two levels below the last intact vertebral arch (figs. 8B and 8C). In two of the seven patients, there was abrupt transition from a vertebra with intact vertebral arch to the subjacent vertebra with widely bifid laminae. There was no intervening vertebra with narrow spina bifida. In these two patients, the upper end of the hernia ostium and point of cord herniation were one level below the last intact vertebral arch (fig. 4B). One of the seven patients showed a prolonged transition with two narrowly bifid vertebrae interposed between the last intact vertebral arch and the most cephalic, widely bifid laminae. In this patient, the upper end of the hernia ostium and point of cord herniation were three levels below the last intact vertebral arch (fig. 5B).

Validity of Our Conception of Lipomyeloschisis

Our understanding of lipomyeloschisis remains very incomplete. The anatomic relations of the "archetype" presented above have not been proved in all details, principally for lack of detailed postmortem material to section transversely. We do believe that the surgical and radiographic findings in this study document a spectrum of transition between intact and widely bifid neural arches; a constant fibrovascular band stretched between the most cephalic, widely bifid laminae; kinking of the herniating meningocele and spinal cord/placode by that band; bulging of the meningocele to the side opposite the lipoma; constant, intimate relations between the lipoma and the *dorsal* surface of placode; rotation of the herniating placode by the lipoma; constant origin of the ventral and dorsal nerve roots from the ventral surface of the placode (not lipoma); constant course of these roots through the subarachnoid space (not the lipoma) to their exit foramina; and complete absence of any lipoma within the subarachnoid space.

Laboratory evidence (fig. 1) documents that the dura is reflected onto the ipsilateral dorsal root entry zones, creating a dorsal dural deficiency in the chicken embryo with mechanically induced spina bifida. Surgical experience (figs. 4C and 6C) strongly suggests that this also occurs in humans with lipomyelomeningocele.

Review of the literature provides additional support for these concepts and indicates that the features observed in the patients in our series are representative of those to be expected in any series of patients with lipomyeloschisis. Bruce and Schut [6] and McLone et al. [27] detected skin appendages and dermal sinuses, as illustrated in figure 8, in 7% and 12% of all lumbosacral lipomas, respectively. Lassman and James [19] and Gold et al. [13] observed spina bifida in every case of lumbosacral lipoma. Sacral deformities, as illustrated in figures 7 and 9, have been reported in up to 50% of patients with lumbosacral lipomas [10, 32]. Anomalous bony protrusions (fig. 7), which arise from or articulate with the inferomedial aspect of the ilium at the sacroiliac joint and extend inferiorly to narrow the greater sciatic notch, appear to be infrequent but typical concomitants of lumbosacral lipoma [5, 21, 26, 35, 36, 41].

Dubowitz et al. [10] appreciated the presence and significance of the transverse fibrovascular band and illustrated its relation to the kinked cord, placode, and lipoma (their fig. 1). Anderson [3] also illustrated the transverse band in a schematic diagram of lipomyelomeningocele (his fig. 1A). Blaauw [53] noted a fibrous band 3–7.5 mm long, which bridged a defect in the posterior arch of the atlas in 70% of patients with myelomeningocele (not lipoma). This band contained abundant elastic tissue, was distinct from the

surrounding tissue, and attached firmly to the club-shaped free ends of the posterior arch of the atlas. Such bands may be analogous to those seen in the lumbar region of patients with lipomyelomeningocele.

Lassman and James [19] noted the frequency with which meningoceles bulge to the side opposite the lipoma and concluded that "lipomas which extend away from the midline to one side are more likely to contain a meningocele or a myelocele."

Swanson and Barnett [35] and Yashon and Beatty [39] recognized that the lipoma extends deeply, passing through a defect in the dura, not by infiltrating the dura, but these authors did not discuss the relations of the dura to the placode. Leveuf [22] clearly appreciated the true relations among the dura, pia-arachnoid, dorsal root entry zones, dorsally cleft cord (i.e., placode), and lipoma. Leveuf noted that the cord, conus, and nerve roots coursed through the subarachnoid space and illustrated these relationships beautifully in transverse section in his figure 58B (reproduced here as fig. 1C) [22]. Discussing the "fibro-osseous fissure" in the spinal column at the site of lipoma (i.e., the associated spina bifida), Leveuf stated: "The fissure is well closed in many cases by fibrous tissue that is of dura mater which, coming out of the spinal canal, invaginates inside to terminate in the region of the placode. At this point, the cord is adherent to the deep portion of the lipoma. . ." (author's translation).

Chapman [8] also noted that the dura is reflected onto the lateral edge of the placode posterior to the dorsal nerve roots in cases in which the lipoma inserts onto the posterior surface of the placode. He states that the exact relationship of the dural reflection and lipoma to the dorsal and ventral nerve roots becomes variable when the lipoma inserts more distally onto the caudal termination of the conus [8]. This has not been our experience to date.

Histologic studies [11, 22, 38] document that the lipoma itself is unremarkable and is composed of ordinary adult fat cells (infrequently, brown fat or mixed yellow and brown fat). Smooth and striated muscle fibers, angiomatous elements, calcification, and ossification commonly accompany the lipoma [11, 22, 38]. Atypical features, found in up to 23% of cases, include ependyma-lined canals at the lipal/neural junction reminiscent of the terminal ventricle [54], islands of neuroglia with large neurons at the lipal/neural junction, and intralipal meningeal and enteric cysts with collagenous or smooth muscle walls and clear or chocolate colored fluid contents [22, 38]. Degeneration of lipoma to malignant teratoma and adenocarcinoma is extremely rare [24, 28].

The precise nature of the lipal/neural interface remains debatable. In the chicken embryos, the lipal/neural interface becomes indistinct along the dorsal columns of the cord. In this region, lipoma, fibrous tissue, and neural structures become intermixed. The neural structures involved, however, are the fibers traversing the dorsal columns deep to the dorsal root entry zones, not the dorsal nerve roots themselves. Confusion about the true dorsal nerve roots in the subarachnoid space, the dorsal root entry zones, and the nerve fibers in dorsal columns is believed to account for some of the conflicting reports concerning the presence of nerve roots within the lipoma and of lipoma within the cord [11, 22, 29]. Midline surgical approaches that dissect directly downward toward the dorsal face of placode compound the difficulty since the surgeon comes upon neural tissue precisely at the dorsal columns and the complex fibrous tissue at the dorsal lipal/neural interface (vide infra). Other accounts of "nerve roots" traversing the lipoma may well represent mistakes in identifying as nerve roots those *spinal nerves* that have already exited the subarachnoid space and that may, therefore, normally traverse the epidural fat.

Unfortunately, detailed, modern histologic analysis of the lipal/neural interface in humans is not available. Postmortem material is limited [15, 16, 22, 25], and surgical specimens rarely include the dorsal columns at the deep surface of lipoma [11]. The best pathologic descriptions available are those of Leveuf [22] (*conal lipomyelocele*) and Ehni and Love [11] (*thoracic intradural lipoma*).

Leveuf noted that the cord and central canal above the lipoma were normal, except in two cases with syringomyelia [22]. At the level of the placode and lipoma (fig. 1C), the ventral horns were normal, gave rise to normal ventral roots, and were separated by a normal ventral median sulcus containing the anterior spinal artery [22]. Partial dorsal myeloschisis created a placode with two dorsal hemicords, each of which gave rise to ipsilateral dorsal nerve roots. Thickened pia mater containing smooth muscle fibers covered the ventral and lateral surfaces of the cleft cord [22].

The dorsal cleft was not lined by ependyma; all traces of the ependymal central canal had disappeared. Rather, the cleft was lined by a relatively thick layer of connective tissue that contained smooth muscle fibers and islands of neuroglia [22]. This connective tissue is the homologue of the fibrous subareolar tissue seen in other types of spina bifida [22]. The dorsal surface of the connective tissue layer was covered by the lipoma into which it sent irregularly shaped projections. These were densest near the neural placode and progressively less dense toward the superficial surface of the lipoma [22]. At its superficial surface, the lipoma was diffuse and continued without transition into the adipose tissue of the surrounding skin [22].

Caudal to the level of the placode, the neural tissue reconstituted a closed spinal cord with central canal and a filum terminale in at least some cases [22]. The lipoma occasionally extended into this part of cord [22].

Ehni and Love [11] reported the pathology of a 20-year-old woman with a midthoracic intradural lipoma which was inseparable from cord (case 2). A V-shaped longitudinal strip biopsy taken along the most prominent meridian of the lipoma included a small part of the dorsal columns of the cord. In this specimen, the neural tissue was separated from lipoma by a heavy, irregular layer of connective tissue that contained islands of fat and cord tissue as well as myelinated nerves with hyperplastic endoneurium. No fat lay bare within or adjacent to the cord. The little fat "within" the cord was enclosed by the cellular connective tissue. Fat-containing projections of this connective tissue invariably passed deeply into the dorsal surface of cord. Connective tissue

projections also extended superficially into the lipoma and decreased progressively in density toward the superficial surface of lipoma. A fibrous capsule of moderate thickness ensheathed the lipoma.

Surgical Procedure and Presurgical Neuroradiologic Evaluation

It is believed that lipomyeloschisis causes neurologic dysfunction in two ways: (1) progressive deposition of fat within each of the static number of fat cells results in increased intracanalicular mass effect in the absence of mitosis and (2) the lipomatous mass tethers the cord, resulting in stretching of the cord, especially during growth spurts. The goal of surgery, then, is to reduce the bulk of fatty intracanalicular mass and to untether the cord. Because the normal state of the cord is to be bathed by subarachnoid fluid, it is considered desirable to reconstruct surgically a closed neural and arachnoid tube in order to approximate as closely as possible the natural environment of the cord. Such reconstruction also reduces the risk of postsurgical scarring and consequent retethering of cord and placode to canal by scar tissue.

Proper presurgical radiologic assessment of lipomyeloschisis requires a working knowledge of the surgical procedure to be performed, its risks, and the way to minimize those risks by accurate display of anatomy. To that end, the procedure for repair and untethering of lipomyeloschisis is illustrated in figure 6 and summarized briefly in the caption.

Until the surgeon has entered the subarachnoid space and identified the nerve roots visually, he has no direct knowledge of the locations of the vulnerable nerve roots buried deep to his scalpel. However, serial CT images at 5 mm (or other) fixed intervals from above the last intact arch down through the sacrum enable the surgeon to know the precise structures at each point simply by using a ruler to measure the distance in the patient from the last palpably intact arch to the point of interest and then counting down the appropriate number of CT images.

Plain spine radiographs and metrizamide CT myelography document the presence and site of spina bifida, the size and symmetry of the widely bifid laminae, the presence of lipomyeloschisis, the side and size of the lipoma, the degree of cephalic extension of lipoma within the extraarachnoid space and within the central canal of the cord, the side and size of the bulging subarachnoid space, the position of the tethering fibrovascular band, the degree of rotation of the herniating placode, the consequent relation of the dorsal root entry zones to the midline, and the courses and lengths of the dorsal and ventral nerve roots.

Radiographic display of a lipomyeloschisis with typical features signifies a high likelihood of achieving successful untethering of the spinal cord. Conversely, display of unusual features associated with a lipomyeloschisis signals increased difficulty at surgery and decreased likelihood of achieving complete untethering of the cord. For example, an anomalous dorsal sacroiliac bony keel (fig. 7) may easily be mistaken for a lamina at surgery, leading to tedious, fruitless dissection outside the true spinal canal. Irregularity and indistinctness of the dorsal lipal/neural interface on CT (figs. 8D–8F) suggest the presence of complicating elements that may well prevent successful untethering of the cord. Unusually short intraarachnoid segments of the nerve roots (fig. 8G) suggest potential difficulty in untethering the cord, since such short roots may prevent complete relaxation and ascent of the cord despite successful dissection of the conus from the lipoma and the filum terminale. In these latter cases, however, it is believed that the degree of tension may diminish with nerve growth as the patient ages, unless postsurgical scarring retethers the cord at another site. Finally, patients with aberrant sacroiliac joints, sacral scoliosis, sacral defects, and/or confluent sacral neural foramina (fig. 10) are predisposed to tethering of the conus by unusually short ipsilateral nerve roots extending between the conus and the aberrant foramina.

In our experience, plain spine radiographs and high-resolution metrizamide CT myelography are the most important and, probably, the sole necessary radiographic examinations for precise preoperative evaluation of the patient with lipomyeloschisis. Metrizamide CT myelograms provide the surgical road map for determining the safest, most efficient: (1) line of approach to the lesion; (2) identification of the first widely bifid vertebra; (3) resection of the intralaminal fibrous band that tethers the placode at the level of the most cephalic, widely bifid laminae; (4) entrance into the canal; (5) durotomy precisely over the meningocele; (6) visualization of the placode and emerging roots through the arachnoid; (7) entry into the meningocele under direct vision, sparing the dorsal nerve roots at their entry zone into placode; (8) establishment of the subarachnoid planes around the lesion; (9) trimming of the lipoma from the dorsal surface of placode; and (10) reestablishment of the dural tube over the placode to ensure lateral freedom from tethering. The combination of high-resolution CT, microsurgical technique, and intraoperative monitoring of neural function by evoked potentials has so decreased operative morbidity [27] that we now believe all lipomeningoceles should be treated in the neonatal period before the onset of symptoms. Later treatment will stabilize neurologic deficit, and may be associated with significant neurologic improvement, but rarely achieves return to normal neurological status.

Conclusions

We have not elucidated the mechanism by which lipomeningoceles form, nor have we explained the occurrence of intradural lipoma in some of the patients, and lipomyelomeningoceles in others. We have not resolved reports of nerve roots traversing the walls of the spina bifida during part of their course [22] and absence of any such observations in this series. We have not yet established whether the striking similarity between the normal avian glycogen body and human lipomyeloschisis is trivial coincidence or evidence for a common embryogenesis. However, the entire conception, as advanced herein, accords very well with our experience in vivo and has aided us materially in planning

successful surgery for this condition. We believe, therefore, that the conception advanced will serve, at least, as a working hypothesis and paradigm for lipomyeloschisis.

ACKNOWLEDGMENTS

We thank Carol Fabian, Carol Freda, Olga Guzman, Tracy Kolbas, Arthur Nieves, Ernesto Salazar, Jr., and Gloria Short for their assistance in manuscript preparation; David Weil of Kascot Media for photographic assistance; and Andrew K. Poznanski (Chicago) and Dominique Marton (Montreal) for translation of Leveuf's work.

REFERENCES

1. Emery JL, Lendon RG. Lipomas of the cauda equina and other fatty tumours related to neurospinal dysraphism. *Dev Med Child Neurol [Suppl]* **1969**;11:62–70
2. Ammerman BJ, Henry JM, De Girolami U, Earle KM. Intradural lipomas of the spinal cord: a clinicopathological correlation. *J Neurosurg* **1976**;44:331–336
3. Anderson FM. Occult spinal dysraphism: diagnosis and management. *J Pediatr* **1968**;73:163–177
4. Barry JF, Harwood-Nash DC, Fitz CR, Byrd DW. Metrizamide in pediatric myelography. *Radiology* **1977**;124:409–418
5. Bassett RC. The neurologic deficit associated with lipomas of the cauda equina. *Ann Surg* **1950**;131:109–116
6. Bruce DA, Schut L. Spinal lipomas in infancy and childhood. *Childs Brain* **1979**;5:192–203
7. Caram PC, Scarcella G, Carton CA. Intradural lipomas of the spinal cord with particular emphasis on the "intramedullary" lipomas. *J Neurosurg* **1957**;14:28–42
8. Chapman PH. Congenital intraspinal lipomas: anatomic considerations and surgical treatment. *Childs Brain* **1982**;9:37–47
9. Dossetor RS, Kaiser M, Veiga-Pires JA. CT scanning in two cases of lipoma of the spinal cord. *Clin Radiol* **1979**;30:227–231
10. Dubowitz V, Lorber J, Zachary RB. Lipoma of the cauda equina. *Arch Dis Child* **1965**;40:207–213
11. Ehni G, Love JG. Intraspinal lipomas: report of cases; review of the literature, and clinical and pathologic study. *Arch Neurol Psychiatry* **1945**;53:1–28
12. Guiffre R. Intradural spinal lipomas: review of the literature (99 cases) and report of an additional case. *Acta Neurochir* (Wien) **1966**;14:69–95
13. Gold LHA, Kieffer SA, Peterson HO. Lipomatous invasion of the spinal cord associated with spinal dysraphism: myelographic evaluation. *AJR* **1969**;107:479–485
14. James HE, Oliff M. Computed tomography in spinal dysraphism. *J Comput Assist Tomogr* **1977**;1:391–397
15. Johnson A. Fatty tumour from the sacrum of a child, connected with the spinal membranes. *Trans Pathol Soc Lond* **1857**;8:16–18
16. Johnson A. Fatty tumour connected with the interior of the spinal canal of the sacrum. *Trans Pathol Soc Lond* **1857**;8:28–29
17. Kaiser MC, Pettersson H, Harwood-Nash DC, Fitz CR, Armstrong E. Direct coronal CT of the spine in infants and children. *AJNR* **1981**;2:465–466
18. Kaplan JO, Quencer RM. The occult tethered conus syndrome in the adult. *Radiology* **1980**;137:387–391
19. Lassman LP, James CCM. Lumbosacral lipomas: critical survey of 26 cases submitted to laminectomy. *J Neurol Neurosurg Psychiatry* **1967**;30:174–181
20. Lemire RJ, Graham CB, Beckwith JB. Skin-covered sacrococcygeal masses in infants and children. *J Pediatr* **1971**;79:948–954
21. Lester PD, McAlister WH. Congenital iliac anomaly with sciatic palsy. *Radiology* **1970**;96:397–399
22. Leveuf J. *Spina bifida avec tumeur*. Paris: Masson et Cie, **1937**:75–88
23. Lohkamp R, Claussen C, Schuhmacher G. CT demonstration of pathologic changes of the spinal cord accompanying spina bifida and diastematomyelia. *Prog Pediatr Radiol* **1978**;6:200–227
24. Love JG. Delayed malignant growth of a congenital teratoma with spina bifida: case report. *J Neurosurg* **1968**;29:532–534
25. Mallory TB, Castleman B, Parris EE. Case records of the Massachusetts General Hospital: case 34131. *N Engl J Med* **1948**;238:443–448
26. McAlister WH, Siegel MJ, Shackelford GD. A congenital iliac anomaly often associated with sacral lipoma and ipsilateral lower extremity weakness. *Skeletal Radiol* **1978**;3:161–166
27. McLone DG, Mutluer S, Naidich TP. Lipomeningoceles of the conus medullaris. In: *American Society for Pediatric Neurosurgery: concepts in pediatric neurosurgery III*. Basel: Karger (in press)
28. Mickle JP, McLennan JE. Malignant teratoma arising within a lipomeningocele: case report. *J Neurosurg* **1975**;43:761–763
29. Naidich TP, McLone DG, Palacio CA. Presurgical evaluation of lipomyelomeningoceles. Presented at the annual meeting of the American Society of Neuroradiology, Chicago, April **1981**
30. Resjo IM, Harwood-Nash DC, Fitz CR, Chuang S. Computed tomographic metrizamide myelography in spinal dysraphism in infants and children. *J Comput Assist Tomogr* **1978**;2:549–558
31. Rogers HM, Long DM, Chou SN, French LA. Lipomas of the spinal cord and cauda equina. *J Neurosurg* **1971**;34:349–354
32. Roller GJ, Pribram HFW. Lumbosacral intradural lipoma and sacral agenesis. *Radiology* **1965**;84:507–511
33. Scatliff JH, Bidgood WD Jr, Killebrew K, Staab EV. Computed tomography and spinal dysraphism: clinical and phantom studies. *Neuroradiology* **1979**;17:71–75
34. Schroeder S, Lackner K, Weiand G. Lumbosacral intradural lipoma. *J Comput Assist Tomogr* **1981**;5:274
35. Swanson HS, Barnett JC Jr. Intradural lipomas in children. *Pediatrics* **1962**;29:911–926
36. Theander G. Malformation of the iliac bone associated with intraspinal abnormalities. *Pediatr Radiol* **1975**;3:235–239
37. Villarejo FJ, Blazquez MG, Gutierrez-Diaz JA. Intraspinal lipomas in children. *Childs Brain* **1976**;2:361–370
38. Walsh JW, Markesbery WR. Histological features of congenital lipomas of the lower spinal canal. *J Neurosurg* **1980**;52:564–569
39. Yashon D, Beatty RA. Tethering of the conus medullaris within the sacrum. *J Neurol Neurosurg Psychiatry* **1966**;29:244–250
40. Wolpert SM, Scott RM, Carter BL. Computed tomography in spinal dysraphism. *Surg Neurol* **1977**;8:199–206
41. Cohen JY, Lebatard-Sartre R, Lajat Y, Mitard D, David A. Sacral intraspinal lipoma associated with congenital iliac anomaly. *Childs Brain* **1981**;8:181–188
42. Ethier R, King DG, Melancon D, Belanger G, Taylor S, Thompson C. Development of high resolution computed tomography of the spinal cord. *J Comput Assist Tomogr* **1979**;3:433–438
43. Dryden R. The fine structure of spina bifida in an untreated three-day chick embryo. *Dev Med Child Neurol [Suppl]* **1971**;13:116–124
44. Fowler I. Responses of the chick neural tube in mechanically

produced spina bifida. *J Exp Zool* **1953**;123:115–151
45. Romanoff AL. The avian embryo: structural and functional development. New York: Macmillan, **1960**;212–309
46. Watterson RL. Development of the glycogen body of the chick spinal cord: I. Normal morphogenesis, vasculogenesis and anatomical relationships. *J Morphol* **1949**;85:337–390
47. Watterson RL. Development of the glycogen body of the chick spinal cord: III. The paired primordia as revealed by glycogen-specific stains. *Anat Rec* **1952**;113:29–52
48. Bulcke JA, Termote JL, Palmers Y, Crolla D. Computed tomography of the human skeletal muscular system. *Neuroradiology* **1979**;17:127–136
49. Osborn AG, Koehler PR. Computed tomography of the paraspinal musculature: normal and pathologic anatomy. *AJR* **1982**;138:93–98
50. Chiu LC, Schapiro RL. A primer in computed axial tomographic anatomy: II. The lower abdomen and female pelvis. *CT* **1977**;1:137–144
51. Schapiro RL, Chiu LC. A primer in computed axial tomographic anatomy: III. The male pelvis. *CT* **1977**;1:213–218
52. Warkany J, Wilson JG, Geiger JF. Myeloschisis and myelomeningocele produced experimentally in the rat. *J Comp Neurol* **1958**;109:35–54
53. Blaauw G. Defect in posterior arch of atlas in myelomeningocele. *Dev Med Child Neurol [Suppl]* **1971**;12:113–115
54. Kernohan JW. The ventriculus terminalis: its growth and development. *J Comp Neurol* **1924**;38:107–125